Self-calibration of PIV video-cameras in Scheimpflug condition

T. Fournel [†], J.-M. Lavest [††], S. Coudert [†], F. Collange [††]

[†] LTSI, UMR CNRS 5516, 10 rue Barrouin, 42000 Saint-Etienne, France
[††] LASMEA, UMR CNRS 6602, 63177 Aubière cedex, France

Abstract

In order to introduce more flexibility in calibration, the bundle adjustment approach is introduced for Stereo PIV systems in Scheimpflug condition. The calibration target is positionned by hand front of the video-cameras at different locations in space. From the multiple views of the calibration target, the parameters of the video-cameras with both the target locations and the 3D calibration points are estimated by non linear least mean squares. In the proposed calibration procedure, the laser plane equation is determined by searching for the homography between the image planes. The ability of the procedure for self-calibrating two f=50 mm video-cameras and recovering the equation of the measurement plane is experimentally tested.

1. Introduction

Stereo Particle Image Velocimetry technique (SPIV) enables instantaneous velocity field measurements in various situations. Whatever are the stereoscopic set-up and the possible optical interfaces, the evaluation of the three velocity components in a section of the flow is based on the function mapping any 3D location to its image. The mapping function modeling one video-camera is classically a polynomial function (Van Oord 1997) or an homographic one (Raffel et al. 1998) whose parameters are recovered at the calibration stage from 3D well-known points and their correspondences in the image plane. Usually a known flat grid is placed in the median plane of the light sheet and accurately moved to different locations parallel to the light sheet (Soloff et al. 1997). At each location, images of the grid are recorded. Such a calibration method may be unstable relative to non parallel and not equally spaced target locations, especially in internal flows (e.g. pipe flow). It is the reason why (Quénot et al. 2001) proposed

a method using a single image of a dot grid target to calibrate a PIV video-camera with the focal length and sensor pixel pitches as additional information. Nowadays multi-level targets on which different z-positions are present are available for the special case of SPIV calibration (Naqwi 2000). Such an object has to be accurately defined and carefully handled during and after the experiment. In addition, a series of 3D calibration targets is required to inspect a large range of fields, from microPIV fields to aerodynamics ones.

The aim of this article is to obtain an easier PIV calibration protocol by hand-positioning a printed flat calibration target. In computer vision, such a *self-calibration* based on the bundle adjustment techniques (Lavest et al. 1998, Triggs et al. 2000) already works in applications using a zoom (Li and Lavest 1996, De Agapito et al. 2001) or inspections with a very short focal length. In this multi-plane and photogrammetrical approach described in section 2, one requires neither a remote control translation nor an accurate calibration target : the video-camera intrinsic parameters and the calibration target geometry are recovered simultaneously. In section 3, we propose two intrinsic models consistent with the specific case of the Scheimpflug condition used in the SPIV angular method. The problem of misalignment is tackled in section 4 where the localization of the laser plane is carried out in the calibrated stereo device coordinate system. Compared to other work on the topic (Riou 1999, Bjorkquist 1998, Coudert and Schon 2001), we propose to determine the homography between both image planes when imaging the laser plane. In order to validate the approach and to assess its precision, displacements of the flat dot grid used for the self-calibration of two $f = 50\,mm$ video-cameras in Scheimpflug condition were measured (section 5). The ability of the laser plane localization method has been tested on a target with a printed random dot pattern.

2. The bundle adjustment approach

2.1. Self-calibration from multiple images

The bundle adjustment technique is a least mean square method used in computer vision for self-calibrating video-cameras from a calibration target. This technique is based on a multi-image scheme leading to a highly over-determined non-linear system and a reliable estimation of both the intrinsic parameters of the video-cameras and the 3D calibration points. In such a photogrammetric approach, extrinsic parameters giving the localization of one video-camera, are distinguished from the intrinsic parameters.

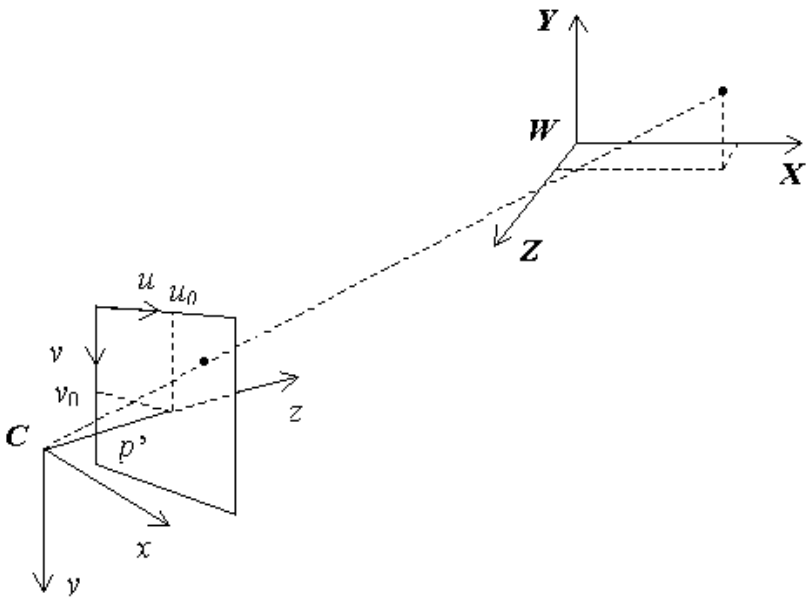

Fig. 1. The pin-hole camera model, image geometry and coordinate systems.

Let us consider the *pin-hole* model depicted in figure 1 where the *convention of the painter* has been adopted (i.e. the image plane is placed front of the projection centre in order to work with a positive value for magnification). This is a simplified model of the left (or the right) video-camera assumed to work according to a perspective projection. To first order, the relationship between a 3D point given in the reference coordinate system $W-XYZ$ and its image in the video-camera coordinate system $C-XYZ$ is described by the following equations :

$$\begin{pmatrix} x \\ y \\ p' \end{pmatrix} = \lambda \left[\mathrm{R} \begin{pmatrix} x \\ y \\ p' \end{pmatrix} + \mathrm{t} \right] \tag{2.1}$$

where p' is the distance separating the projection centre from the image plane (denoted p' in figure 1), $\boldsymbol{R} = \left(r_{ij}\right)$ and $\boldsymbol{t} = \left(t_x, t_y, t_z\right)^T$ are respectively the rotation matrix and the translation vector between the world and video-camera coordinate systems. By eliminating in (2.1) the scale factor λ which maps the 3D point to its image, one obtains the following so-called *collinearity equations* :

$$x = p' \frac{r_{11}X + r_{12}Y + r_{13}Z + t_x}{r_{31}X + r_{32}Y + r_{33}Z + t_z}$$
$$y = p' \frac{r_{21}X + r_{22}Y + r_{23}Z + t_x}{r_{31}X + r_{32}Y + r_{33}Z + t_z} \tag{2.2}$$

By taking into account distortions $(\delta x, \delta y)$, the coordinates (x, y) are transformed into the pixel coordinate (u, v) as follows :

$$x + \delta x = (u + \varepsilon_u - u_0)dx$$
$$y + \delta y = (v + \varepsilon_v - v_0)dy \tag{2.3}$$

where $\varepsilon_u, \varepsilon_v$ are the errors on the image location (u, v) measured in the pixel array, (u_0, v_0) are the pixel coordinates of the intersection between the optical axis and the image plane, (dx, dy) the pixel sizes. Distortions are usually divided in two parts, on one hand the radial distortions given by the parameters a_1, a_2, a_3, on the other hand the tangential ones given by the parameters p_1, p_2 (ASP 1984) :

$$\delta x_r = (u - u_0)(a_1 r^2 + a_2 r^4 + a_3 r^6)dx$$
$$\delta y_r = (v - v_0)(a_1 r^2 + a_2 r^4 + a_3 r^6)dy \tag{2.4}$$

$$\delta x_t = \left[p_1 \left(p_x{}' r^2 + 2\frac{(u-u_0)^2}{p_x'} \right) + 2p_2 (u-u_0)\frac{v-v_0}{p_y'} \right] dx$$
$$\delta y_t = \left[p_2 \left(p_y{}' r^2 + 2\frac{(v-v_0)^2}{p_y'} \right) + 2p_1 \frac{u-u_0}{p_x'}(v-v_0) \right] dy \tag{2.5}$$

where $p'_x = \frac{p'}{dx}$ and $p'_y = \frac{p'}{dy}$ represent the image distances expressed in pixel unit and $r = \sqrt{\frac{(u-u_0)^2}{p_x'^2} + \frac{(v-v_0)^2}{p_y'^2}}$ is the radial distance from the image centre.

Substituting (2.3), (2.4) and (2.5) into (2.2), the measurement errors can be expressed as

$$\varepsilon_u(\boldsymbol{\Phi}) = u_0 + p_x{}' \frac{r_{11}X + r_{12}Y + r_{13}Z + t_x}{r_{31}X + r_{32}Y + r_{33}Z + t_z} + \frac{\delta x_r + \delta x_t}{dx} - u$$
$$\varepsilon_v(\boldsymbol{\Phi}) = v_0 + p_y{}' \frac{r_{21}X + r_{22}Y + r_{23}Z + t_x}{r_{31}X + r_{32}Y + r_{33}Z + t_z} + \frac{\delta y_r + \delta y_t}{dy} - v \tag{2.6}$$

where $\boldsymbol{\Phi}$ is the vector of unknown parameters. The vector $\boldsymbol{\Phi}$ is estimated by minimizing the sum $\sum_{i=1}^{n} \left({\varepsilon_{u_i}}^2 + {\varepsilon_{v_i}}^2 \right)$ from the n points $\left(X_i, Y_i, Z_i\right)_{i=1,\ldots,n}$ of a flat calibration grid and their images $\left(u_i, v_i\right)_{i=1,\ldots,n}$ localized in the pixel array. At this stage, the parameter vector $\boldsymbol{\Phi}$ consists of intrinsic and extrinsic parameters of the video-camera. By looking at (2.4), (2.5), (2.6) and by keeping in mind that a perspective projection is always defined within a scale factor, the image distances p'_x and p'_y appear as intrinsic parameters. The image centre coordinates $\left(u_0, v_0\right)$ and the optical distortion parameters a_1, a_2, a_3, p_1, p_2 are the other ones. The extrinsic parameters are the three *independent* rotation angles of the rotation $\boldsymbol{R}$ (α rotating around X-axis, β around Y-axis, and γ around Z-axis) and the translation vector $\boldsymbol{t} = \left(t_x, t_y, t_z\right)^T$. Thus, the parameter vector, denoted here $\boldsymbol{\Phi}_{9+6}$, is

$$\Phi_{9+6} = \left(u_0, v_0, p'_x, p'_y, a_1, a_2, a_3, p_1, p_2, \alpha, \beta, \gamma, t_x, t_y, t_z\right)^T$$

One major source of calibration errors is the result of measurement errors. These errors can be located on the 3D coordinates of the calibration target points but also on the localization of their correspondences in the image plane. One way to improve this is to combine more than one image taken by the same video-camera but from m different views (after rotation given by Euler's angles $\alpha^{(k)}, \beta^{(k)}, \gamma^{(k)}$ and/or translation given by ${t_x}^{(k)}, {t_y}^{(k)}, {t_z}^{(k)}$). In such a case, the intrinsic parameters remain the same for all the images and the calibration task means computing the following parameter vector :

$$\boldsymbol{\Phi}_{9+6m} = (u_0, v_0, p'_x, p'_y, a_1, a_2, a_3, p_1, p_2, \alpha^{(1)}, \beta^{(1)}, \gamma^{(1)}, {t_x}^{(1)}, {t_y}^{(1)}, {t_z}^{(1)}, \ldots, \alpha^{(m)}, \beta^{(m)}, \gamma^{(m)}, {t_x}^{(m)}, {t_y}^{(m)}, {t_z}^{(m)})^T$$

It has been proved that measurements with a subpixel accuracy (2/100 pixel) can be obtained with special patterns like crosses or dots. In that case, the major source of calibration errors relies on calibration patterns.

High quality calibration patterns are difficult to achieve. They have to be mechanically stable in time (compared with the temperature change) or to be moved very accurately to insure an euclidian reference frame without bias.

Taken into account this point of view, it has been demonstrated that it is possible inside a multi-image calibration approach to estimate the calibration point coordinates together with the intrinsic and extrinsic calibration parameters.

The new parameter vector to be determined, if the coordinates $X^{(i)}, Y^{(i)}, Z^{(i)}$ of the n calibration points have to be estimated with the traditional calibration parameters, takes the following form:

$$\begin{aligned}\Phi_{9+6m+3n} = \big(&u_0, v_0, p'_x, p'_y, a_1, a_2, a_3, p_1, p_2,\\ &\alpha^{(1)}, \beta^{(1)}, \gamma^{(1)}, t_x{}^{(1)}, t_y{}^{(1)}, t_z{}^{(1)},\\ &\ldots, \alpha^{(m)}, \beta^{(m)}, \gamma^{(m)}, t_x{}^{(m)}, t_y{}^{(m)}, t_z{}^{(m)},\\ &X^{(1)}, Y^{(1)}, Z^{(1)}, \ldots, X^{(n)}, Y^{(n)}, Z^{(n)}\big)^T\end{aligned} \tag{2.7}$$

where n represents the total number of target points and m the total number of images taken during the calibration stage.

Figure 2 shows the classical set of views used during calibration. The video-camera is rotated around the target to insure a cone of observation views and introduce geometrical constrains in the 3D computation of calibration points. Note that rotating the camera around the object is identical to rotate the object around a fixed camera.

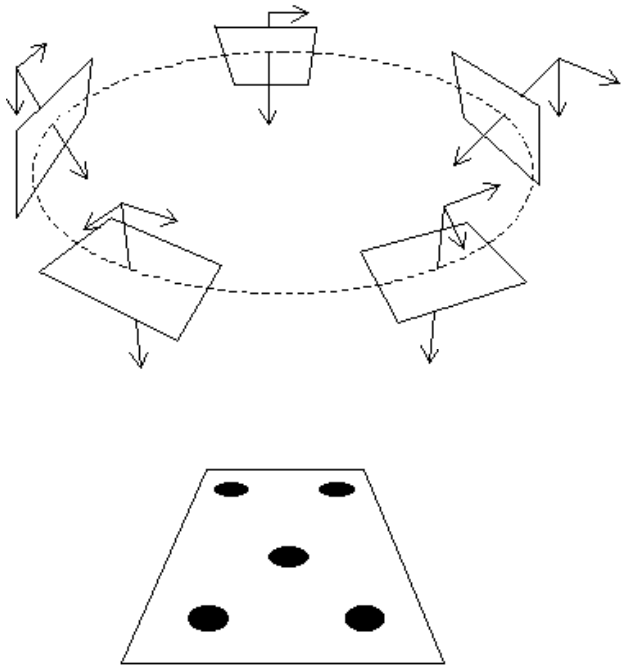

Fig. 2. Classical camera geometry during self-calibration sequence.

2.2. Solving the Problem

The errors ε_u and ε_v being non-linear functions of $\boldsymbol{\Phi}$, the minimization of (2.6) is a non-linear optimization problem. One way of solving the problem is to

linearize (2.6) with some initial value $\boldsymbol{\Phi}_0$ and solve for $\boldsymbol{\Delta\Phi}$. The solution is then obtained by adding $\boldsymbol{\Delta\Phi}$ to $\boldsymbol{\Phi}_0$ as the new initial value and repeating the process until a certain convergence is satisfied.

Given n 3D points and their corresponding 2D image points in m views, we can write the $2 \times n$ linearized measurement or error equations in matrix form:

$$\boldsymbol{V} = \boldsymbol{L} + \boldsymbol{A}\boldsymbol{\Delta\Phi} \tag{2.8}$$

with $\boldsymbol{L} = \boldsymbol{\varepsilon}\left(\boldsymbol{\Phi}_0\right)$ and $\boldsymbol{A} = \nabla\boldsymbol{\varepsilon}\left(\boldsymbol{\Phi}_0\right)$.

Let the weight matrix of the measurements be $\boldsymbol{W}$, the least squares solution to (2.8) is a minimization problem of

$$\min_{\Delta\Phi\in\Re^{9+6m+3n}}\left(\mathrm{V}^T\mathrm{W}\mathrm{V}\right) \tag{2.9}$$

The solution to (2.9) can be obtained as:

$$\boldsymbol{\Delta\Phi} = \left(\boldsymbol{A}^T\boldsymbol{W}\boldsymbol{A}\right)^{-1}\left(\boldsymbol{A}^T\boldsymbol{W}\boldsymbol{L}\right) \tag{2.10}$$

From the least square estimate of (2.8) and (2.9), we can compute the estimate of the residual vector $\boldsymbol{V}$ as

$$\hat{\mathrm{V}} = \left(\mathrm{I} + \mathrm{A}\left(\mathrm{A}^T\mathrm{W}\mathrm{A}\right)^{-1}\mathrm{A}^T\mathrm{W}\right)\mathrm{L} \tag{2.11}$$

the estimate of the so called *standard error of unit weight*, which is the a posteriori estimate of the standard deviation σ_0 of the noise on the image coordinates if the model is correct and there are no system errors:

$$\hat{\sigma}_0^2 = \frac{\boldsymbol{V}^T\boldsymbol{W}\boldsymbol{V}}{N-r} \tag{2.12}$$

and the estimate of the *covariance* matrix of the parameters $\boldsymbol{\Phi}$:

$$\boldsymbol{C}_{\boldsymbol{\Phi}} = \left(\boldsymbol{A}^T\boldsymbol{W}\boldsymbol{A}\right)^{-1} \tag{2.13}$$

For each individual parameter Φ_i, we can then compute the estimate of its precision, or the standard deviation:

$$\hat{\sigma}_i^2 = \hat{\sigma}_0^2 c_{ii} \tag{2.14}$$

In order to assure algorithm convergence, the calibration vector set as initial value has to be not too far from the solution. In the final experimental results, we will show that this initial value is not really difficult to obtain, and that a good convergence can be achieved if the calibration views of the pattern are taken from

different orientation observations. This is equivalent to insuring very constrained triangulation angles in space for the 3D point reconstruction. As underlined in (Brown 1971), we have noticed that multiple views taken with a $\pm$ 45 degree rotation around the object leads to a better estimate (better convergence and better accuracy) of the calibration parameters.

Since the 3D coordinates of the calibration points are simultaneously estimated with the calibration parameters, the extrinsic geometry of the vision system is determined up to a scale factor. Actually, in these conditions the reconstruction of a bigger calibration pattern observed from a farther distance will provide an identical image. This loss of metric dimensions does not have great consequences on a single video-camera calibration. Key information for further application tasks are only contained in the intrinsic parameters. Let us recall that extrinsic parameters give the 3D location of the calibration pattern, expressed in the video-camera frame, and in accordance with a given view of the image set. In order to calibrate with two (or more) video-cameras, it will be necessary to introduce a metric dimension to fix the extrinsic geometry of the video-camera configuration. Such a task can easily be performed with the accurate knowledge of the Euclidian distance between only 2 points among n, or the absolute length of a translation between two views.

3. Scheimpflug model

In angular SPIV, each sensor is tilted according the Scheimpflug condition in order to focus on the laser plane with a low aperture number (Hinsch et al. 1993, Prasad and Jensen 1995). The Scheimpflug condition is obtained as the planes supported by the sensor respectively the lens intersect with the laser plane in a common line. It is depicted in figure 3 with the "painter convention". As sensors are no longer orthogonal to the optical axis, optical distortions are no more isotropic with respect to the image centre.

The general expression for the image coordinates can be obtained by projecting the distorted image coordinates $\left(x+\delta x(x,y), y+\delta xy(x,y), p'\right)$ in the front image plane onto the tilted image plane :

$$\begin{pmatrix} s\tilde{x} \\ s\tilde{y} \\ s \end{pmatrix} = \begin{pmatrix} p'r_{S_{33}} & 0 & 0 & 0 \\ 0 & p'r_{S_{33}} & 0 & 0 \\ 0 & 0 & 1 & 0 \end{pmatrix} \begin{pmatrix} \boldsymbol{R}_{Sch} & \boldsymbol{0} \\ 0 & 1 \end{pmatrix} \begin{pmatrix} x+\delta x \\ y+\delta y \\ p' \\ 1 \end{pmatrix} \tag{3.1}$$

where the Scheimpflug rotation $\boldsymbol{R}_{Sch}$ defines the rotation from the video-camera coordinate system to the tilted image plane coordinate system.

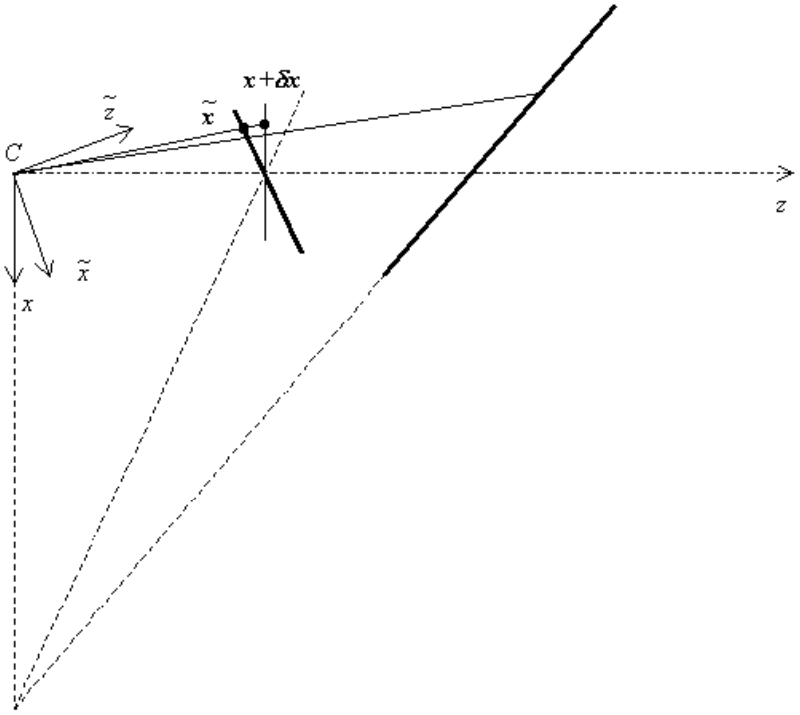

Fig. 3. Scheimpflug condition according to the "painter convention" (the "image" plane is placed front of the projection centre by symmetry of the optical image plane with respect to the projection centre).

When the distortions and measurement errors due to the sub-pixel pattern detector are of the same order of magnitude, the Scheimpflug rotation is compensated with the extrinsic rotation that defines the object plane position in the video-camera frame. According to a perspective point of view, this is not a real problem. Indeed calibration defines the sensor and the object in space, and in that case the classical projection scheme has to be choosen.

Remember that no accuracy is required both in the flat calibration target definition and in its displacement, because all these parameters will be estimated during the non linear optimization. In section 5 we will use a planar calibration object printed by a laser printer and manually moved to create the set of images.

4. Laser plane equation

After calibration of the stereo system, the rigid transformation $(\boldsymbol{R}_S, \boldsymbol{t}_S)$ from the second video-camera coordinate system to the first one for the i^{th} view is given by :

$$\begin{pmatrix} R_i^{(1)} & \boldsymbol{t}_i^{(1)} \\ 0 & 1 \end{pmatrix} = \begin{pmatrix} R_S & \boldsymbol{t}_S \\ 0 & 1 \end{pmatrix} \begin{pmatrix} R_i^{(2)} & \boldsymbol{t}_i^{(2)} \\ 0 & 1 \end{pmatrix} \tag{4.1}$$

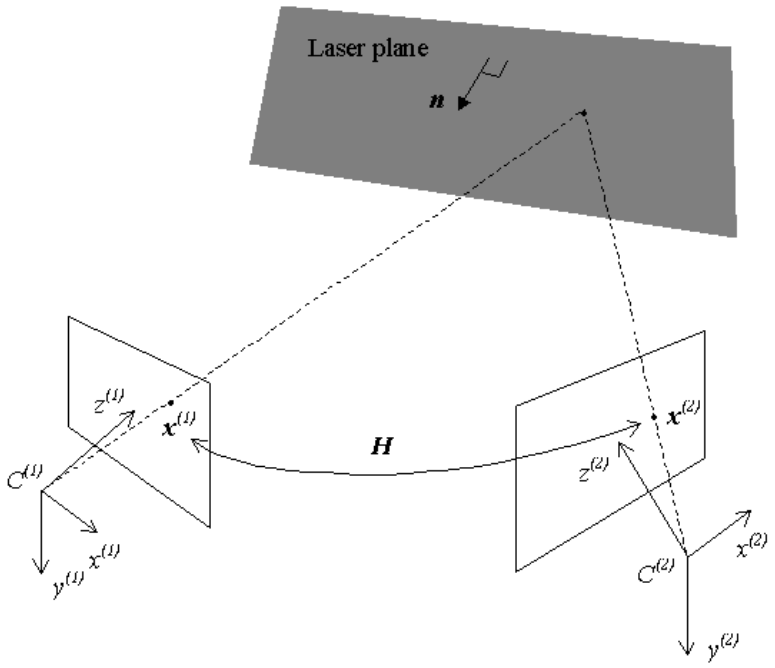

Fig. 4. Homography transformation between images when viewing the laser plane.

Let us assume that the optical distortions are corrected. As the projections are perspective ones, there exists a pure homography transformation $\boldsymbol{H}$ between points $\boldsymbol{x}^{(1)}$ (of pixel homogeneous coordinates $\boldsymbol{u}^{(1)} = \left(u^{(1)}, v^{(1)}, 1\right)^T$) and $\boldsymbol{x}^{(2)}$ (of pixel homogeneous coordinates $\boldsymbol{u}^{(2)} = \left(u^{(2)}, v^{(2)}, 1\right)^T$) (Hartley and Zisserman 2000) :

$$s\,\boldsymbol{u}^{(2)} = \boldsymbol{H}\,\boldsymbol{u}^{(1)} \tag{4.2}$$

where $\boldsymbol{H}$ is a 3 by 3 matrix defined with only 3 unknown parameters and s a scalar introduced in order to normalize the third component of $\boldsymbol{u}^{(2)}$. In fact, the image $\boldsymbol{u}^{(2)}$ is the image of the back-projection of $\boldsymbol{u}^{(1)}$ on the laser plane. The laser plane being defined by the distance d from the first projection centre and by the normal vector $\boldsymbol{n} = \left(n_x, n_y, n_z\right)^T$, the homography $\boldsymbol{H}$ can be expressed as :

$$\mathrm{H}=\begin{pmatrix} p_x'^{(2)} & 0 & u_0^{(2)} & 0 \\ 0 & p_y'^{(2)} & v_0^{(2)} & 0 \\ 0 & 0 & 1 & 0 \end{pmatrix} \begin{pmatrix} \mathrm{R}_S & \mathrm{t}_S \\ 0 & 1 \end{pmatrix} \begin{pmatrix} 1 & 0 & 0 & 0 \\ 0 & 1 & 0 & 0 \\ 0 & 0 & 1 & 0 \\ \frac{n_x}{d} & \frac{n_y}{d} & \frac{n_z}{d} & 0 \end{pmatrix} \begin{pmatrix} \frac{1}{p_x'^{(1)}} & 0 & -\frac{u_0^{(1)}}{p_x'^{(1)}} \\ 0 & \frac{1}{p_y'^{(1)}} & -\frac{v_0^{(1)}}{p_y'^{(1)}} \\ 0 & 0 & 1 \\ 0 & 0 & \frac{1}{p'^{(1)}} \end{pmatrix} \tag{4.3}$$

The purpose is to find the three unknowns $\left(a,b,c\right)^T = \frac{1}{d}\boldsymbol{n}$ which leads to the laser plane equation. The solution $\left(\tilde{a},\tilde{b},\tilde{c}\right)^T$ can be obtained by minimizing the sum $\sum_{i=1}^{2mn} \boldsymbol{\varepsilon}_i^T \boldsymbol{\varepsilon}_i$ where $\boldsymbol{\varepsilon}_i$ is the deviation vector between the measured position $\boldsymbol{u}_i^{(2)}$ (corresponding to the i^{th} measured position $\boldsymbol{u}_i^{(1)}$) and the current value $\frac{1}{s}\boldsymbol{H}_{a,b,c}\boldsymbol{u}_i^{(1)}$.

5. Experimental results

The method proposed for SPIV self-calibration has been applied on a pair of 1024 × 768 1/2" CCD cameras mounted on the Scheimpflug devices designed by the Laboratory of Mechanics of Lille (France) in the frame of the Europiv 2 project. The CCD cameras were equipped with *f*=50mm lenses focused on the measurement plane with a distance of 500 mm and viewing it at 45°. For self-calibration, we have a total number of 9+6*m*+3*n* unknown parameters (included intrinsic and extrinsic parameters and also calibration point coordinates from (2.7)) for 2*mn* equations. By using 25 calibration dots on a flat support observed from 8 views i.e. 400 measurements for 132 unknown parameters, the system to be solved is clearly redundant. The views are taken by hand-positioning the flat calibration target according to very different orientations (± 45°) in order to better estimate the calibration parameters.

The Scheimpflug video-cameras have been self-calibrated according to a classical projection scheme (section 3) as distortions appeared negligible in displacement measurements carried out in this experiment. The coordinates of the image centre are (498,320) pixel in frame 1 and (680,570) pixel in frame 2. The values of p'_x and p'_y (maintained equal as pixels are square) are 8206 pixel for video-camera 1 and 8210 pixel for video-camera 2. They corresponds to an object distance of 470 mm. The rigid transformation of the stereo device $(\boldsymbol{R}_S, \boldsymbol{t}_S)$ (which allows to pass from the second video-camera coordinate system to the first one) is given on table 1. The calibration parameter vector has been obtained with absolute residuals less than 0.04 pixel.

Table 1. Rigid transformation of the stereo device.

α	β	γ	t_x	t_y	t_z
+68.42°	+86.82°	+69.72°	-499.56 mm	-26.55 mm	+467.74 mm

Table 2. Translation measurements in translation motion.

α (°)	β (°)	γ (°)	t_x (mm)	t_y (mm)	t_z (mm)	Angle (°)	Magnitude (mm)
0.0011	0.0016	-0.0002	0.9992	0.0145	-0.0145	0.0019	0.9994
0.0009	0.0003	0.0000	1.0012	0.0143	-0.0158	0.0010	1.0014
0.0001	0.0007	-0.0001	0.9993	0.0151	-0.0163	0.0007	0.9995
-0.0001	0.0011	0.0003	0.9987	0.0144	-0.0144	0.0011	0.9990
0.0013	0.0014	0.0003	0.9975	0.0141	-0.0132	0.0019	0.9977
0.0016	0.0018	0.0002	0.9989	0.0144	-0.0143	0.0024	0.9991
0.0005	0.00155	0.0006	0.9974	0.0142	-0.0148	0.0017	0.9976
0.0005	0.0016	-0.0003	0.9996	0.0144	-0.0140	0.0017	0.9998
0.0005	0.0012	0.0005	1.0004	0.0141	-0.0142	0.0014	1.0006
-0.0003	0.0017	-0.0001	1.0016	0.0144	-0.0158	0.0017	1.0018
0.0011	0.0007	-0.0001	0.9990	0.0151	-0.0156	0.0013	0.9992
0.0001	0.0013	0.0002	0.9996	0.0142	-0.0143	0.0013	0.9998
0.0012	0.0022	0.0003	0.9980	0.0140	-0.0130	0.0026	0.9982
0.0007	0.0010	0.0005	0.9984	0.0141	-0.0137	0.0013	0.9986
0.0005	0.0014	0.0001	0.9982	0.0142	-0.0145	0.0015	0.9984
0.0004	0.0010	0.0004	0.9997	0.0140	-0.0140	0.0012	0.9999
0.0006	0.0011	0.0000	1.0018	0.0142	-0.0132	0.0013	1.0020
0.0003	0.0002	-0.0006	1.0011	0.0145	-0.0139	0.0007	1.0013
Mean							0.9996
Deviation							0.0013

In order to assess the precision of this calibration, the flat calibration target was mounted on remote control stages. The target was first translated along the horizontal *X*-axis in the object plane with a 1 mm step and secondly rotated around the Y-vertical axis by -0.5° steps. For each location, the position of each dot was

measured by the self-calibrated stereo device using the sub-pixel pattern detector then the target plan localised. The rotation-translation transformation between the k^{th} and $(k+1)^{th}$ positions of the target expressed in the k^{th} target coordinate system is reported in table 2 for the translation motion (20 samples) and in table 3 for the rotation motion (8 samples). The motions have been recovered within 2 µm for the translation and within 0.003° for the rotation, which agrees with the resolution of the remote control stages.

The method proposed in section 4 for recovering the laser plane equation has been tested on a randomly-printed paper sticked on a CD-ROM by way of support and positioned in front of the calibrated stereo device. The method applied on the whole images of the stereo pair gave the equation of the support plane in 31 iterations. Figure 5 shows the ability of the method which has detected a small bump at the location of the central hole of the CD-ROM. 2225 points defined in frame 1 were matched with their corresponding points in frame 2 by correlation. Afterwards the corresponding 3D points were reconstructed by triangulation (in the coordinate system of video-camera 1). The mean distance of the 3D points from the recovered plane is less than 7 µm and the standard deviation equal to 93 µm.

Table 3. Displacement measurements in rotation motion.

α (°)	β (°)	γ (°)	t_x (mm)	t_y (mm)	t_z (mm)	Angle (°)	Magnitude (mm)
0.0082	-0.4970	0.0048	-0.1842	0.0003	-0.2566	0.4971	0.3158
0.0080	-0.5003	-0.0059	-0.1831	0.0006	-0.2570	0.5004	0.3156
0.0088	-0.5026	-0.0070	-0.1832	0.0007	-0.2578	0.5028	0.3163
0.0080	-0.4983	-0.0077	-0.1805	0.0005	-0.2548	0.4984	0.3122
0.0048	-0.5015	-0.0050	-0.1851	0.0007	-0.2604	0.5015	0.3195
0.0075	-0.5011	-0.0058	-0.1838	0.0005	-0.2587	0.5012	0.3173
0.0071	-0.5038	-0.0067	-0.1843	0.0006	-0.2593	0.5039	0.3181
Mean						0.5008	
Deviation						0.0022	

6. Conclusion

We have demonstrated that the calibration of an angular Stereo PIV system in Scheimpflug condition can be performed by hand-positioning a paper-printed target and recording a set of views. After detecting the target marks in the views, an optimal pin hole model is searched for as the same time than the localization of the views and the coordinates of the marks on the target by non linear least mean square. We showed that the misalignment problem can be solved by searching for the homography between the two image planes when viewing the measurement plane. Such a protocol has been evaluated in air on synthetic objects.

After self-calibrating the experimental set-up, displacements were measured within a precision close to the resolution of the remote control devices used in multi-plane calibration. The method proposed for the recovery of the measurement plane equation allowed to detect a bump of a few of micrometers. The redundancy for self-calibrating can be increased by replacing the localization of the second

roposed
. will be
rame of

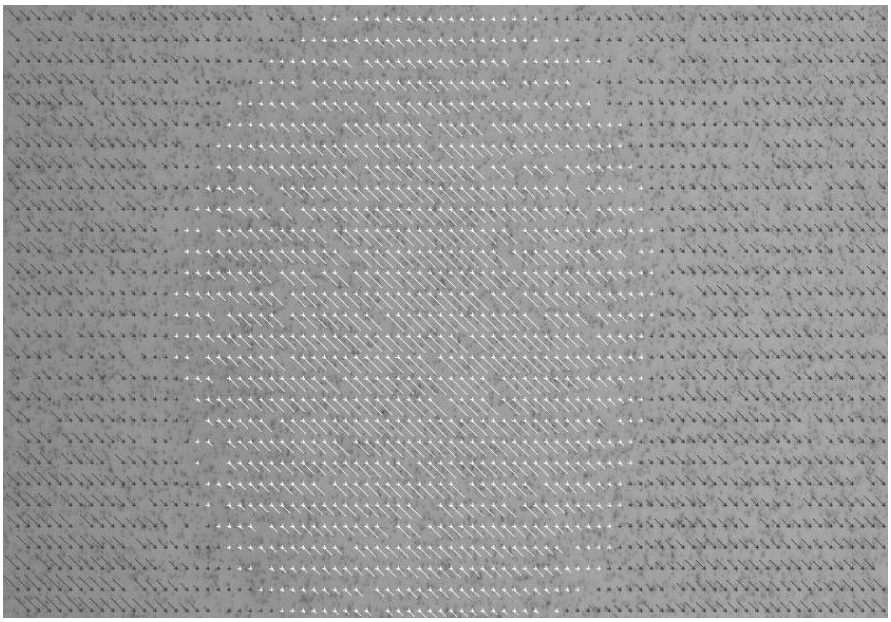

Fig. 5. Vectors from the recovered plane to the measured points over-printed on the random pattern (equation of the paper plane recovered in the coordinate system of video-camera 1 : $0.7005X-0.0224Y-0.7134Z+347.09=0$).

References

American Society for Photogrammetry (1984) Manual of Photogrammetry. Fourth edition

Bjorkquist D.C. (1998) Design and calibration of a stereoscopic PIV system. Ninth International Symposium on Applications of Laser Techniques to Fluid Mechanics, Lisbon, Portugal, July 13-16

Brown D.C. (1971) Close-range camera calibration. Photogrammetric Engineering 37:8**:**855-866

Coudert S., Schon J.P. (2001) Back projection algorithm with misalignment

corrections for 2D3C stereoscopic PIV. Meas. Sci. and Technol. 12:1371-1381
De Agapito L., Hayman E., Reid I. (2001) Self-calibration of rotating and zoo ming cameras. Int. Journal of Computer Vision 45:2
Fournel T., Coudert S., Fournier C., Ducottet C. (2003) Stereoscopic particle image velocimetry using telecentric lenses. Meas. Sci. and Technol. 14:494-499
Hartley R., Zisserman A. (2000) Multiple view geometry in computer vision. Cambridge University Press
Hinsch K.D., Hinrichs H., Roshop A., Dreesen F. (1993) Holographic and steros copic advances in 3-D PIV. Holographic Particle Image Velocimetry. Proc. of Fluids Engineering Division, American Society of Mechanical Engineers, ed. E.P. Rood 148:33-36
Lavest J.M., Viala M., Dhome M. (1998) Do we really need an accurate calibration pattern to achieve a reliable camera calibration. Proc. of ECCV98, Freiburg, Germany, 158-174
Li M., Lavest J.M. (1996) Some aspects of zoom lens calibration. IEEE PAMI 18:11
Prasad A.K., Jensen K. (1995) Scheimpflug stereocamera for particle image velocimetry in liquid flows. Applied Optics 34:7092-7099
Naqwi A. (2000) Distortion compensation for PIV systems. Tenth International Symposium on Applications of Laser Techniques to Fluid Mechanics, Lisbon, Portugal
Quénot G., Rambert A., Lusseyran F., Gougat P. (2001) Simple and accurate PIV camera calibration using a single target image and camera focal length. Fourth International Symposium on Particle Image Velocimetry, Göttingen, Germany, September 17-19, paper 1040
Raffel M., Willert C., Kompenhans J. (1998) Particle Image Velocimetry : A practical guide. 3rd edition, Springer, ISBN 3-540-63683-8
Riou L. (1999) Methods of calibration of a stereoscopic system for 2D and 3D flow velocity field measurements. Thesis, Saint-Etienne University, France
Soloff S., Adrian R., Liu Z.C. (1997) Distortion compensation for generalised stereoscopic particle image velocimetry. Meas. Sci. and Technol. 8 :1441-1454
Triggs W., McLauchlan P., Hartley R., Fitzgibbon A. (2000) Bundle adjustment: a modern synthesis. LNCS W.Triggs, A.Zisserman, R.Szeliski, Eds. Springer Verlag
J. Van Oord (1997) The design of a stereoscopic DPIV system. Report MEAH-161 Delft the Netherlands: Delft University of Technology